ACS APPLIED MATERIALS & INTERFACES

Research Article

www.acsami.org

Large-Area Preparation of High-Quality and Uniform Three-Dimensional Graphene Networks through Thermal Degradation of Graphene Oxide–Nitrocellulose Composites

Xin Zhang,*[,†] Katherine S. Ziemer,[∥] Kun Zhang,[§] Donald Ramirez,[‡] Li Li,[§] Shiren Wang,[§] Louisa J. Hope-Weeks,[‡] and Brandon L. Weeks*[,†]

[†]Department of Chemical Engineering, [‡]Department of Chemistry & Biochemistry, and [§]Nanomaterials and Nanomanufacturing Laboratory, Department of Industrial Engineering, Texas Tech University, Lubbock, Texas 79409, United States

[∥]Department of Chemical Engineering, Northeastern University, Boston, Massachusetts 02115, United States

Supporting Information

ABSTRACT: We demonstrate a simple method to prepare high-quality and uniform three-dimensional (3D) graphene networks through thermal degradation of graphene oxide (GO)–nitrocellulose composites over a large area. The nitrocellulose simultaneously acts as a support and aids in the reduction of GO by exothermic decomposition. The graphene networks have tunable porous morphology where the pore size can be controlled by adjusting the concentration of GO in the composite. This new technique is a very simple method to obtain 3D graphene networks and has the potential to produce 3D graphene-modified substrates for use in energy storage and conversion applications, in supporting frameworks of catalyst, and in sensors. In this report, the prepared 3D graphene networks were directly used as the electrodes of supercapacitors without using a binding agent and/or conducting additive with a high specific capacitance of 162.5 F g^{-1} at 0.5 A g^{-1} current density.

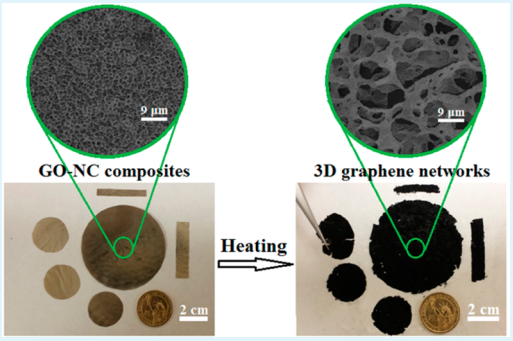

KEYWORDS: *three-dimensional graphene networks, graphene oxide–polymer composites, nitrocellulose, supercapacitor*

INTRODUCTION

Graphene, which is a one-atom thick sheet of carbon, has been widely applied in energy storage and conversion, organic synthesis, catalysis, polymer fabrication, biomedicine, sensors, and micro/nanoelectronics due to its high electronic and thermal conductivity, mechanical strength, optical properties, and large theoretical specific surface area.[1−11] However, these graphene sheets commonly aggregate during processing in solution due to strong $\pi-\pi$ interactions and van der Waals forces making dispersion difficult.[12,13] Aggregation of the graphene sheets reduces the specific surface area, hinders the mass and electron transport, and can adversely affect the thermal and mechanical properties of graphene-based materials.[13−15] Therefore, it is of continuous interest to develop simple, practical, and effective methods to construct graphene networks to avoid aggregation and take full advantage of graphene's intrinsic physical and chemical properties. To date, a series of techniques have been applied to fabricate graphene networks, such as chemical vapor deposition (CVD),[1,16−19] electrochemistry,[14] chemical or thermal reduction of graphene oxide (GO)-based composites,[20−28] self-assembly,[29,30] lithographic patterning,[31] chemical etching,[25] vacuum filtration,[32] and nucleate boiling.[33] Among these methods, CVD and chemical or thermal reduction of GO-based composites appear to be the most effective methods for large-area preparation of high-quality and uniform graphene networks.

CVD is a popular microfabrication process widely used to produce high-purity and large-scale thin films. It has been commercially applied in the semiconductor industry, for example, in the preparation and modification of silicon-based materials. It is also the dominant method for producing carbon nanofibers and carbon nanotubes. CVD has been used for producing graphene networks using metal catalysts such as Cu, Au, and Ni.[1,16−19] However, the CVD process usually uses highly flammable gases for raw carbon sources and typically requires high processing temperatures. In addition, after depositing graphene sheets on a template, extra steps are often required to remove the template. To avoid the collapse of three-dimensional (3D) structured graphene during the template etching, a thin layer of polymer such as poly(dimethylsiloxane) (PDMS) is often deposited to protect the graphene sheets as a support.[16] After etching, the polymeric residue can influence the electrical and thermal properties of graphene.[34,35] Therefore, the CVD process can be high-cost,

Received: June 9, 2014
Accepted: December 19, 2014
Published: December 19, 2014

DOI: 10.1021/am508909h
ACS Appl. Mater. Interfaces 2015, 7, 1057−1064

complex, and time-consuming for the preparation of graphene networks.[36]

Chemical or thermal reduction of GO-based composites is another popular technique for the preparation of graphene networks.[20−28] This technique requires constructing a GO-based composite and then reducing the GO to produce the graphene networks. GO is one of the most important functional graphene materials.[37−39] It is widely studied due to the low cost of preparation and is a well-adopted precursor to synthesis various graphene-based materials through high-temperature thermal reduction,[40] chemical-reagent reduction,[41] or photothermal reduction.[42] In contrast to pure graphene, which is difficult to disperse,[43] GO contains abundant oxygen-containing groups on the basal planes and edges, making it easier to disperse in many organic solvents and water.[37,44] One challenge in making 3D networks is that the chemical or thermal reduction of GO often causes collapse of the pore structure without the use of a support (e.g., polymer or other material), which must be subsequently removed.[12,13,20−28,45−50]

Herein, we report a simple method to fabricate high-quality and uniform 3D graphene networks through thermal degradation of GO−nitrocellulose (NC) composites without the use of an additional support. NC is a low-cost industrial polymer with wide-ranging applications in coatings, filtration, and biological sciences.[51,52] It is also an energetic material fill and remains a leading major ingredient of gunpowder and solid rocket propellant formulation.[53−56] GO is easily dispersed in NC to form a composite material.[57] Unlike other polymers or small molecular compounds, which have been used to construct graphene networks, NC can be rapidly, and fully, decomposed. In addition, the reaction is exothermic simultaneously releasing heat to its surroundings during thermal degradation. Through the thermal degradation of the GO−NC composites, the heat generated from the decomposition of NC can be an efficient in situ method to reduce GO to graphene without additional supports. These 3D graphene networks can be fabricated on different substrates and can be directly used as the electrodes of supercapacitors without using a binding agent and/or conducting additive.

EXPERIMENTAL SECTION

Materials. GO powders were purchased from Graphene Laboratories Inc. (Calverton, NY). NC (4−8% in ethanol/diethyl ether, 11.8−12.2 wt % nitrogen) was purchased from Sigma-Aldrich Inc. NC solution was made to solid films before using by evaporating organic solvents at ambient conditions and drying at 70 °C in a vacuum oven until a constant weight is achieved in air.

Preparation of GO−NC Composites. GO powders were dispersed in deionized water by a tip sonicator (Bandelin Sonoplus) for 60 min to make 3 mg/mL GO−water solution. Solid NC was dissolved in acetone to make 5% (mass concentration) NC−acetone solution. Then different amounts of fresh GO solution were added into the NC−acetone solution and stirred for 6 h at room temperature to make various ratios GO−NC solutions. The various GO−NC composites were made through adding various ratios GO−NC solutions to glass Petri dishes (VWR International) of 7.5 × 7.5 cm and then evaporating solvents at ambient conditions and drying at 70 °C in a vacuum oven until a constant weight is achieved in air.

Transmission Electron Microscopy Analysis. Thermally reduced GO (TMRGO) networks were dispersed in acetone by a tip sonicator (Bandelin Sonoplus) for 10 min. The TMRGO networks for transmission electron microscopy (TEM, Hitachi 8100) observation was prepared by placing drops of the TMRGO acetone suspension onto the carbon-coated copper grid (Ultrathin Carbon Film on Holey Carbon Support Film, 400 mesh, Copper, Ted Pella, Inc.), which was then dried under ambient conditions prior to being introduced into the TEM chamber. The samples were measured by using an acceleration voltage of 60 kV.

Scanning Electron Microscopy Analysis. The morphologies of GO−NC composites and TMRGO networks were examined by Hitachi S570 scanning electron microscopy (SEM). All samples were sputter coated a thin layer of gold prior to them (~5 nm) to ensure good conductivity and imaging.

Atomic Force Microscope Analysis. The thickness of graphene sheets from TMRGO networks were obtained with a Nanoscope IIIa multimode atomic force microscope (AFM, Veeco, Santa Barbara, CA) operating in tapping mode. The AFM tips (Tetra15/Au/15, Nanotechnology LLC.) is a silicon cantilever with Au conductive coating, with the resonant frequency of 200−400 kHz and force constant of 20−75 N/m. All images were collected at a scan rate of 0.5 Hz with a driving frequency of 325 kHz (256 × 256 lines scan). All samples were made by placing drops of the TMRGO acetone suspension onto a silicon substrate (1 cm × 1 cm), and the solvent was then dried using spin-coater with 3000 rpm for 3 min. Polished silicon wafers were purchased from Nova Electronic Materials Ltd. The diced silicon substrates were cleaned by a solution containing 5 parts NH_4OH (20%), 1 part H_2O_2 (30% solution), and 1 part deionized water and heated to 50−70 °C for 3 h, rinsed with deionized water, and dried at 70 °C in N_2 environment. The substrates were stored in desiccators prior to use.

X-ray Photoelectron Spectroscopic Analysis. The X-ray photoelectron spectroscopic (XPS) analysis of pure GO, pure NC films, GO−NC-1, and TMRGO-1 was performed using the PHI 5000 VersaProbe II Scanning Microprobe with the PHI MultiPak Version 9.3 software (Physical Electronics Inc., MN, USA). All spectra were acquired with a monochromatic aluminum X-ray source ($h\nu$ = 1486.6 eV), a 100 μm spot size in point mode, both electron and ion neutralization, and a hemispherical analyzer pass energy of 29.35 eV. All samples were mounted with double-sided copper tape to the XPS sample holder. All spectra were collected at a 45° takeoff angle. Curve fitting of the C 1s and O 1s spectra was performed using a Gaussian−Lorentzian peak shape after performing a Shirley background correction.

Thermogravmetric Analysis. Thermogravmetric analysis (TGA) was carried out in a TGA i 1000 (Instrument Specialist, Inc.). The temperature was raised from 25 to 1000 °C at the rate of 10 °C/min in air or helium (He) atmospheres.

Brunauer−Emmett−Teller Specific Surface Area Analysis. Prior to data collection, samples were degassed for 24 h at 50 °C. The Brunauer−Emmett−Teller (BET) specific surface area of each material was obtained from the N_2 adsorption/desorption isotherms obtained at 77 K on a Nova 4200e model Surface Area Analyzer (Quantachrome Instrument Corp.) The BET specific surface areas were calculated from five data points of the adsorption branch of the isotherm between the relative pressures of 0.05 and 0.3 P/P_0.

Electrical Conductivity Measurements. The van der Pauw method was employed for electrical conductivity measurements. Electrical contacts were made by pressing small indium pellets on the four corners of each sample. The current−voltage (I−V) sweeps were performed using a Keithley 6221 current source and a Keithley 2182A nanovoltmeter. Direct current (DC) was applied from corner 2 to corner 1, and the voltage was measured between corner 3 and corner 4, R_A was calculated as $(V_{3,4}/I_{1,2} + V_{1,2}/I_{3,4})/2$. DC current was applied from corner 3 to corner 2, and the voltage was measured between corner 1 and corner 4, R_B was calculated as $(V_{1,4}/I_{2,3} + V_{2,3}/I_{1,4})/2$. By measuring R_A and R_B, the electrical conductivity can be calculated by the following equation:

$$\sigma = \left[\frac{\pi d}{\ln 2}\cdot\frac{(R_A + R_B)}{2}\cdot f\left(\frac{R_A}{R_B}\right)\right]^{-1}$$

where d is the film thickness and $f(x) = 1/\cosh(\ln(x)/2.403)$ is the correction factor.[58]

Electrochemical Analysis. To study the electrochemical behavior of TMRGO networks, original GO−NC films were deposited on the

DOI: 10.1021/am508909h
ACS Appl. Mater. Interfaces 2015, 7, 1057−1064

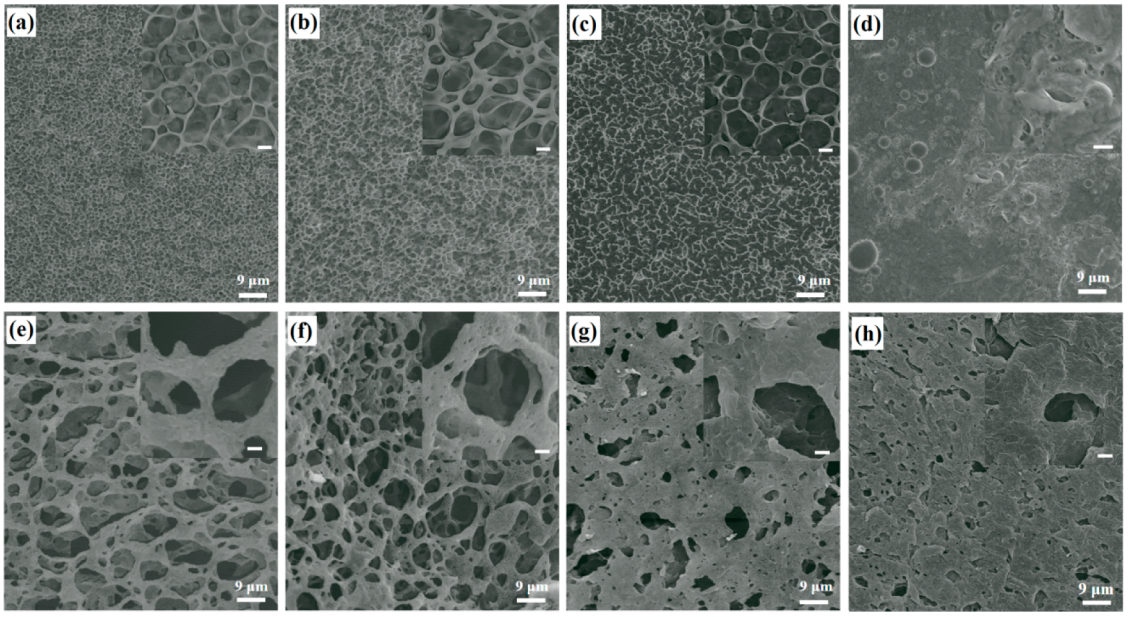

Figure 1. SEM images of GO−NC composites and 3D graphene networks. (a) GO−NC-1, (b) GO−NC-2.5, (c) GO−NC-5, (d) GO−NC-10, (e) TMRGO-1, (f) TMRGO-2.5, (g) TMRGO-5, and (h) TMRGO-10. (inset) Scale bar is 900 nm.

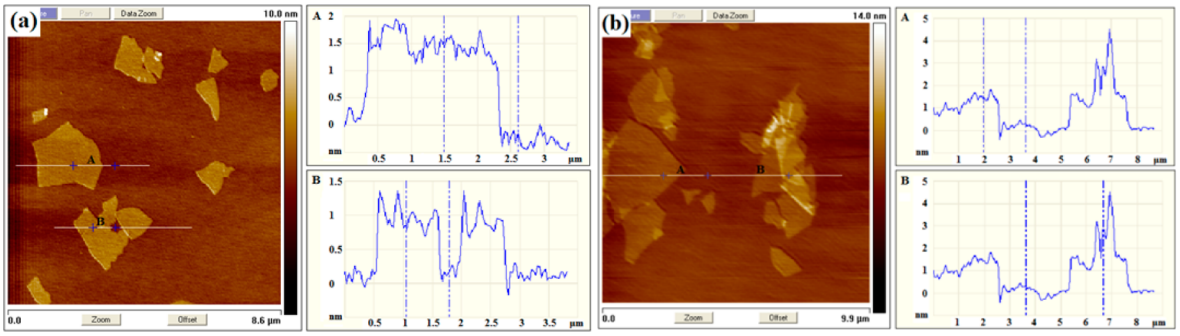

Figure 2. AFM images of graphene sheets from TMRGO networks. (a) TMRGO-1. (b) TMRGO-5.

gold foil and then were heated at 500 °C for 5 min under a helium atmosphere. The electrochemical characterization was carried out on the CHI 660D electrochemical station with a three electrochemical configuration. The TMRGO network on gold foil was used as working electrode, a platinum wire was employed as the counter electrode, and the reference electrode was Ag/AgCl electrode. The 1 M KOH aqueous solution was employed as electrolyte.

RESULTS AND DISCUSSION

Figure 1 represents typical morphologies with various concentrations of GO-doped NC composites as observed by SEM. When introducing 1%, 2.5%, or 5% GO into NC, the morphology of GO−NC composites is formed of highly porous networks, and the pore sizes of these networks are in the range of hundreds of nanometers to several micrometers; see Figure 1a−c. The formation of highly porous networks can be attributed to the interaction forces between NC and GO. The abundant hydroxyl groups and carboxyl groups in GO surface could form hydrogen bonding with nitro groups in NC to allow NC chains connect to GO sheets to form highly porous structures. However, when mixing 10% GO into NC, the pore density is significantly reduced (Figure 1d). After heating the GO−NC composites at 500 °C for 5 min under a helium atmosphere, well-defined and interconnected highly porous 3D networks are obtained (Figure 1e−h). The final weight percentages after reduction (compared to original GO−NC composites) of different 3D networks at 1%, 2.5%, 5%, and 10% GO−NC composites were 0.62 ± 0.11%, 1.58 ± 0.18%, 3.22 ± 0.48%, and 7.96 ± 1.08%. The morphology of these 3D networks is strongly dependent on the GO concentration in original GO−NC composite. With low concentrations of GO (e.g., 1% and 2.5%), the pore sizes of the 3D networks are several micrometers, and the pore walls appear to be graphene sheets. Images of individual sheets with AFM and TEM can be found in Figures 2 and 3.

With higher concentrations of GO (e.g., 5% and 10%), the pore size distribution is in the range of hundreds of nanometers to several micrometers, while the number of pores is reduced significantly. These results indicate that at high GO concentrations, there may be aggregation in the GO−NC composites. To simplify the description, we define 1%, 2.5%, 5%, and 10% GO−NC composites as GO−NC-1, GO−NC-2.5, GO−NC-5, and GO−NC-10, respectively. We also define different 3D graphene networks after thermal degradation as TMRGO-1, TMRGO-2.5, TMRGO-5, and TMRGO-10, with the final number indicating the amount of GO added.

To characterize the specific surface areas (SSA) of different 3D graphene networks, low-temperature nitrogen adsorption measurements were performed. The BET SSAs of TMRGO-1,

DOI: 10.1021/am508909h
ACS Appl. Mater. Interfaces 2015, 7, 1057−1064

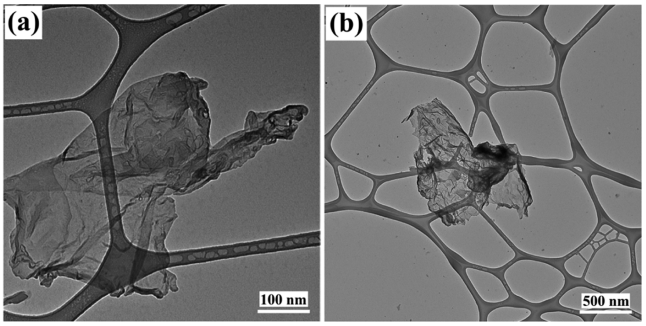

Figure 3. TEM images of graphene sheets from TMRGO networks. (a) TMRGO-1. (b) TMRGO-2.5.

TMRGO-2.5, TMRGO-5, and TMRGO-10 were run in duplicates and measured to be 734/842, 245/305, 44/62, 49/51 $m^2 g^{-1}$, respectively. It can be speculated that all these high SSAs are a result of the highly porous structures formed between ultrathin graphene sheets in TMRGOs. Furthermore, the density of TMRGO-1, TMRGO-2.5, TMRGO-5, and TMRGO-10 were measured to be 3.668 ± 0.635, 6.679 ± 0.875, 9.615 ± 1.337, and 16.864 ± 2.921 mg cm^{-3}, respectively. Because TMRGO-1 had the highest SSA and the lowest density, we focused on this material for further studies.

To determine the chemical nature of the graphene network post-reduction, XPS was carried out to evaluate the composition and chemical bonding of the 3D graphene networks. As seen in Table 1, the thermal treatment reduces both the pure GO and the GO−NC-1 composite leaving 4.3% oxygen remaining in the thermally reduced GO (TMRGO) and 3.0% oxygen remaining the thermally reduced GO−NC-1 (TMRGO-1). In the pure NC film and GO−NC-1, the N atomic composition is 8.5% and 6.5%, respectively. However, there is no observable nitrogen in the TMRGO-1 sample, which indicates NC is completely degraded after heating.

Table 1. Relative Atomic Percent Composition of GO, NC, GO−NC-1, TMRGO-1, and TMRGO

sample	C atomic %	O atomic %	N atomic %
GO	75.1	24.9	
NC	45.2	45.3	8.5
GO−NC-1	49.9	42.1	6.5
TMRGO-1	97.0	3.0	
TMRGO	95.2	4.3	

The XPS carbon and oxygen elemental spectra of pure GO, pure NC film, GO−NC-1, TMRGO-1, and TMRGO are shown in Figure 2, and can help elucidate the differences in morphology from thermally treated GO and thermally treated GO−NC-1 as well as to understand any chemical differences between GO and GO from nitrocellulose. To compensate for charging, all spectra were shifted to a C−C bonding of 284.6 eV. As shown in Figure 4a, the C 1s peak for pure GO contains C−OH and C═O functional groups at the bonding energies of 286.5 and 288.1 eV, respectively,[59,60] as well as the C−C bonding of 284.6 eV. The pure NC and GO−NC-1 films show the C−OH and C−O−NO_2 C 1s bonding peaks located at 286.9 and 288.3 eV, respectively. However, after heat treatment the C 1s spectrum in TMRGO-1 is almost pure C−C bonds and contains a very small peak at 286.5 eV, which can be assigned to residual C−OH bonds.[59,60] This bonding state

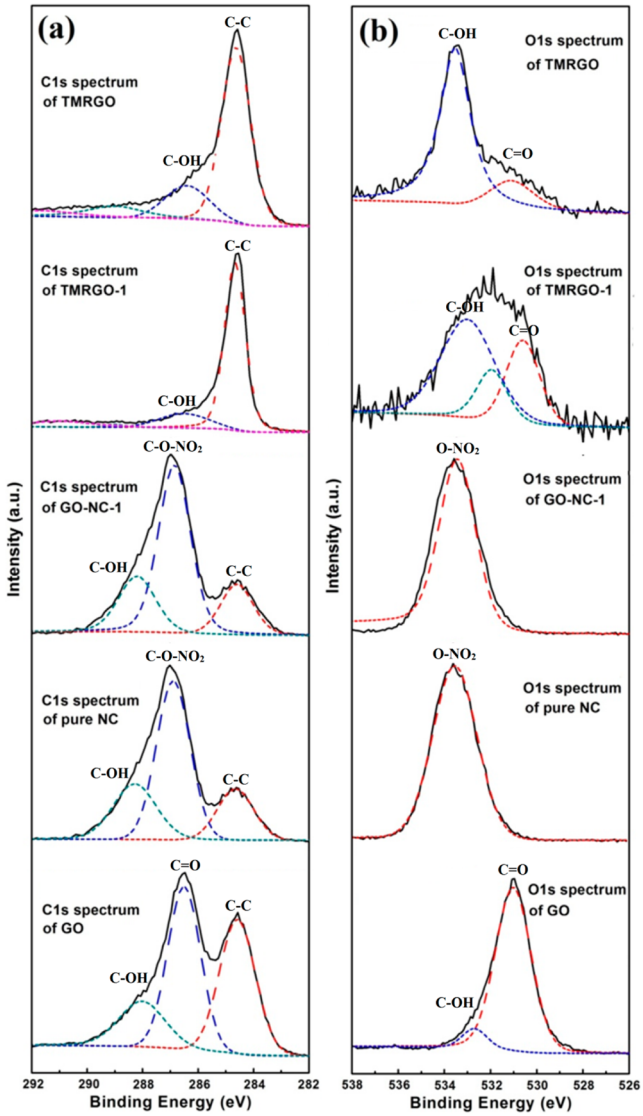

Figure 4. XPS spectra of GO, NC, GO−NC-1, TMRGO-1, and TMRGO. (a) C 1s spectra. (b) O 1s spectra.

change of the C 1s suggests that most of the oxygen-containing groups in original GO sheets are reduced after heating the GO−NC-1 composite, and this is consistent with the change in overall atomic composition. There is no 288.1 eV peak, which indicates all C−O−NO_2 groups are degraded during the heating, again consistent with the overall composition change. The C 1s spectrum in TMRGO also has a small peak at 286.4 eV, which is likely within the uncertainty of C−OH group bonding, and is thus consistent with TMRGO-1.

As shown in Figure 4b, the O 1s peaks are consistent with the carbon peaks in showing the reduction of GO through heating. Pure GO contains C═O and C−OH groups located at 531.0 and 532.7 eV, respectively.[59] The O 1s peak in the pure NC film and GO−NC-1 is located at 533.5 eV and represents the O−NO_2 groups. The O 1s spectrum in TMRGO-1 has some mixed bonding states in the ∼3% of atomic oxygen remaining in the sample. The peak at 530.6 eV is characteristic of C═O groups, which has been observed in reduced graphene oxide.[37] The peak at 533.0 eV is assigned to the C−OH groups.[59] These results also indicate most C═O and C−OH groups on original GO sheets are reduced during heating the

DOI: 10.1021/am508909h
ACS Appl. Mater. Interfaces 2015, 7, 1057−1064

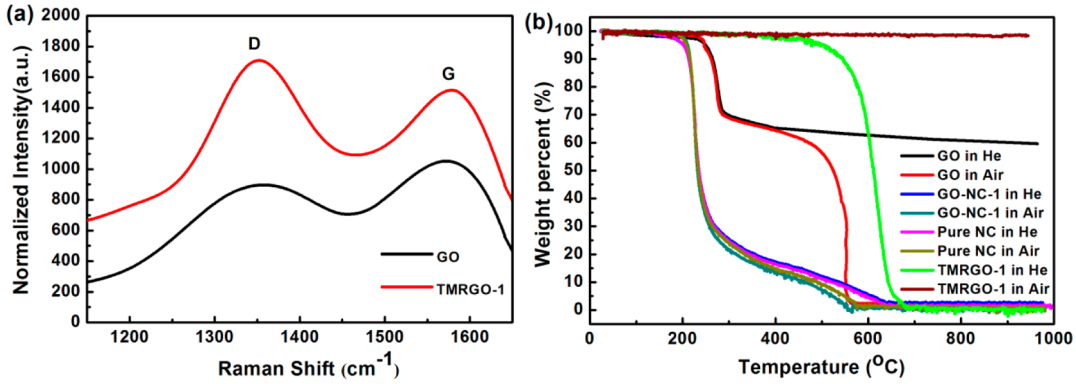

Figure 5. (a) Raman spectra of GO and TMRGO-1 and (b) TGA curves of GO, GO−NC-1, pure NC and TMRGO-1 in He gas and air.

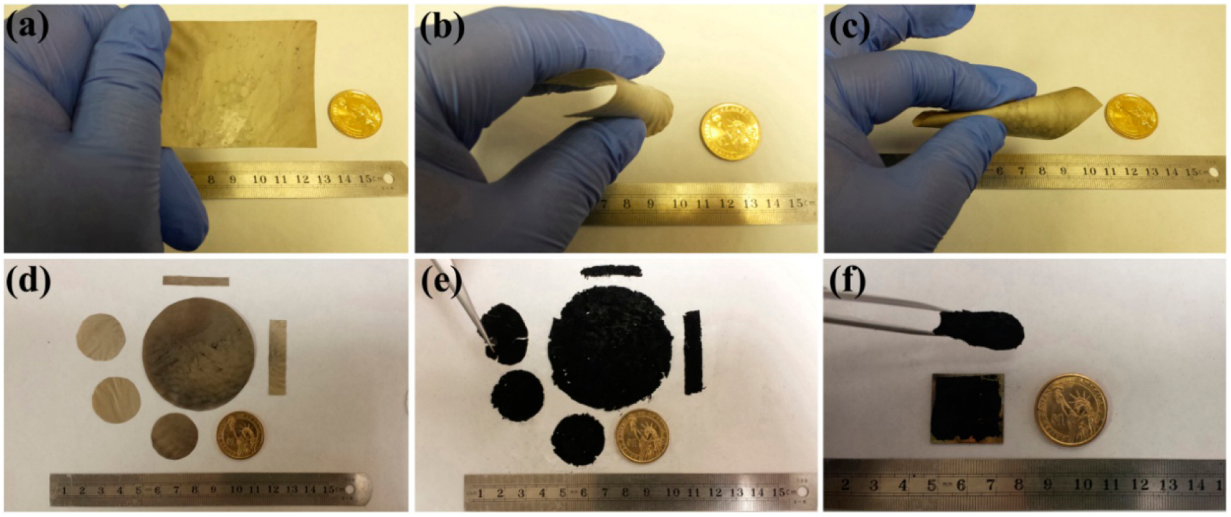

Figure 6. Optical images of GO−NC-1 and TMRGO-1 networks. (a−d) Original GO−NC-1 composites. (e) TMRGO-1 without substrate. (f) TMRGO-1 on ITO/glass (square) and copper substrates.

GO−NC-1 composite. Furthermore, no peak is observed at 533.5 eV, which also indicates that all O−NO_2 groups were decomposed. The O 1s spectrum in TMRGO also has two small peaks at 530.6 and 533.0 eV, which is similar to TMRGO-1 and also supports the conclusion that TMRGO-1 is RGO. Overall, the XPS results clearly demonstrated that thermal degradation of GO−NC composites can produce high-quality 3D graphene networks.

We further investigated the quality of the 3D graphene network using Raman spectra and TGA. The relative intensity of D bands and G band (I_D/I_G) in the Raman spectra for graphene materials reveals the electronic conjugation state.[61,62] As shown in Figure 5a, the Raman spectra show that the ratio of I_D/I_G increased from 0.85 (GO) to 1.14 (TMRGO-1) indicating that GO was reduced during thermal treatment.[61,62] The TGA curves of the pure GO, GO−NC-1, pure NC, and TMRGO-1 are in Figure 5b. Under dry air as a purge gas, pure GO exhibits two onsets for mass loss at 230 and 420 °C, which are attributed to the decomposition of oxygen-containing groups and combustion of graphene sheets, respectively;[40] the GO−NC-1 shows just one mass loss at 200 °C, which is similar to pure NC and is attributed to the decomposition of NC. Subsequent experiments on TMRGO showed a single mass loss at 500 °C indicating the reduced sample is thermally stable up to this temperature and did not contain any residual NC.

TGA experiments were also performed under a He environment. Pure GO shows one mass loss at 230 °C attributed to the reduction step becoming RGO, which is thermally stable up to at least 1000 °C. The TMRGO is thermally stable under He up to 1000 °C, which indicates TMRGO is high-quality RGO.

We demonstrated a simple method to fabricate high-quality and uniform 3D graphene networks through direct thermal degradation of GO−NC composites. The original GO−NC composites are flexible and can be fabricated to the different shapes, as shown in Figure 6a−d; after heating, the shape and size of the 3D networks did not change significantly (Figure 6e). In addition, the thickness of GO−NC composites can be adjusted by controlling the concentration and can also be processed as monoliths (Supporting Information, Figure S1). It is noteworthy to point out that GO−NC composites can be prepared on different substrates, such as indium tin oxide (ITO), various metals, glass, silicon wafers, and even mica. After thermal degradation of the GO−NC composites on these substrates, the 3D graphene networks are still attached to the substrate allowing for further study (Figure 6f).

The TMRGO-1 can be directly used as the electrodes of supercapacitors without using a binding agent and/or conducting additive, and its performance was evaluated by cyclic voltammetry (CV) and galvanostatic charge/discharge. First, the four-probe method was used to measure the electrical

DOI: 10.1021/am508909h
ACS Appl. Mater. Interfaces 2015, 7, 1057−1064

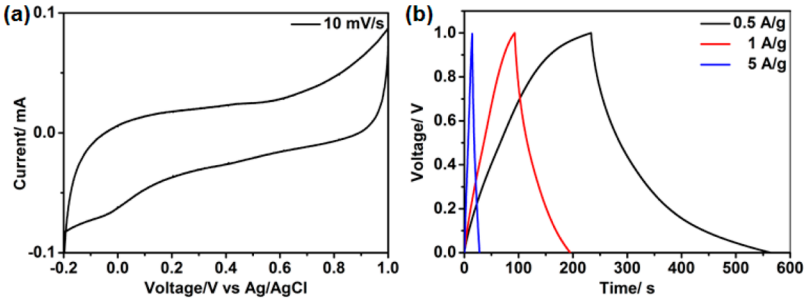

Figure 7. (a) Cyclic voltammograms for the TMRGO-1 that was tested in the 1 M KOH at 10 mV/s; (b) galvanostatic charging/discharging curves measured with different current densities for the TMRGO-1.

conductivity of TMRGO-1, ranging from 1.5 to 5.2 S cm^{-1}. Then CV was employed to study the electrochemical performance of the TMRGO-1, and with the CV curve presented in Figure 7a it can be clearly observed that the as-prepared TMRGO-1 showed a characteristic electric double-layer capacitive behavior, since it not only showed a nearly rectangular curve but also showed no obvious oxidation and reduction peaks, indicating an almost ideal electric double-layer capacitor. Also, the positive and negative scan curves are almost symmetric, which implies the high columbic efficiency of the electrode.

To calculate the specific capacitance of the TMRGO-1, galvanostatic charging/discharging tests were carried out, and the results are presented in Figure 7b. It is suggested that this electrode has excellent electric conductivity, since no obvious IR drops can be found in all of the galvanostatic charging/discharging curves. The specific capacitance can be obtained from the following equation:[63]

$$C_s = \frac{It}{m\Delta V}$$

where C_s is the specific capacitance, I is the charge−discharge current, t is the charge−discharge time, m is the mass of the active material on the electrode, and ΔV is the difference of voltage between beginning and ending of the test. The calculated specific capacitances are 162.5, 105.7, and 68.3 F g^{-1} for the 0.5, 1, and 5 A g^{-1} current densities, respectively. Because the structure of the electrode facilitated the ion transportation, the capacitive retention of the electrode is up to 42% when the current density increased 10 times from 0.5 to 5 A g^{-1}. It is worth mentioning that the columbic efficiencies are 139% at 0.5 A/g^{-1} and 114% at 1 A g^{-1}, indicating that some foreign material also contributes to the capacitance. Given that supercapacitors are usually operated at high current densities, TMRGO-1 has practical applications.

CONCLUSIONS

In conclusion, we have demonstrated a simple method to fabricate high-quality and uniform 3D graphene networks through direct thermal degradation of GO−NC composites. These graphene network assemblies have an open porous structure, and the pore size can be effectively controlled by adjusting the concentration of GO in the NC matrix. In addition, the 3D graphene networks can be fabricated on various substrates and can be directly used as the electrodes of supercapacitors without using a binding agent and/or conducting additive.

ASSOCIATED CONTENT

Supporting Information

Optical images of GO−NC-1 and TMRGO-1 networks. This material is available free of charge via the Internet at http://pubs.acs.org.

AUTHOR INFORMATION

Corresponding Authors

*E-mail: xin.zhang@ttu.edu. (X.Z.)
*E-mail: brandon.weeks@ttu.edu. (B.L.W.)

Notes

The authors declare no competing financial interest.

ACKNOWLEDGMENTS

The authors are grateful for support received from ONR (N00014-11-1-0424) and the U.S. Department of Homeland Security under Award No. 2008-ST-061-ED0001. K.Z., L.L., and S.W. are also grateful to the funding support from National Science Foundation (CMMI No. 1129914 and CMMI No. 0953674).

REFERENCES

(1) Dong, X.; Wang, X.; Wang, L.; Song, H.; Zhang, H.; Huang, W.; Chen, P. 3D Graphene Foam as a Monolithic and Macroporous Carbon Electrode for Electrochemical Sensing. *ACS Appl. Mater. Interfaces* **2012**, *4*, 3129−3133.
(2) Yang, G.; Lee, C.; Kim, J.; Ren, F.; Pearton, S. J. Flexible Graphene-Based Chemical Sensors on Paper Substrates. *Phys. Chem. Chem. Phys.* **2013**, *15*, 1798−1801.
(3) Nardecchia, S.; Carriazo, D.; Ferrer, M. L.; Gutiérrez, M. C.; del Monte, F. Three Dimensional Macroporous Architectures and Aerogels Built of Carbon Nanotubes and/or Graphene: Synthesis and Applications. *Chem. Soc. Rev.* **2013**, *42*, 794−830.
(4) Wang, H.; Yang, Y.; Liang, Y.; Robinson, J. T.; Li, Y.; Jackson, A.; Cui, Y.; Dai, H. Graphene-Wrapped Sulfur Particles as A Rechargeable Lithium-Sulfur Battery Cathode Material with High Capacity and Cycling Stability. *Nano Lett.* **2011**, *11*, 2644−2647.
(5) Huang, X.; Qi, X.; Boey, F.; Zhang, H. Graphene-Based Composites. *Chem. Soc. Rev.* **2012**, *41*, 666−686.
(6) Allen, M. J.; Tung, V. C.; Kaner, R. B. Honeycomb Carbon: A Review of Graphene. *Chem. Rev.* **2010**, *110*, 132−145.
(7) Liu, Y.; Dong, X.; Chen, P. Biological and Chemical Sensors Based on Graphene Materials. *Chem. Soc. Rev.* **2012**, *41*, 2283−2307.
(8) Wu, Z. S.; Sun, Y.; Tan, Y. Z.; Yang, S.; Feng, X.; Mullen, K. Three-Dimensional Graphene-Based Macro- and Mesoporous Frameworks for High-Performance Electrochemical Capacitive Energy Storage. *J. Am. Chem. Soc.* **2012**, *134*, 19532−19535.
(9) Cohen-Karni, T.; Qing, Q.; Li, Q.; Fang, Y.; Lieber, C. M. Graphene and Nanowire Transistors for Cellular Interfaces and Electrical Recording. *Nano Lett.* **2010**, *10*, 1098−1102.

DOI: 10.1021/am508909h
ACS Appl. Mater. Interfaces 2015, 7, 1057−1064

(10) Zhang, X.; Ji, X.; Su, R.; Weeks, B. L.; Zhang, Z.; Deng, S. Aerobic Oxidation of 9H-Fluorenes to 9-Fluorenones using Mono-/Multilayer Graphene-Supported Alkaline Catalyst. *ChemPlusChem* **2013**, *78*, 703−711.
(11) Li, X.; Warzywoda, J.; McKenna, G. B. Mechanical Responses of a Polymer Graphene-Sheet Nano-Sandwich. *Polymer* **2014**, *55*, 4976−4982.
(12) Li, D.; Muller, M. B.; Gilje, S.; Kaner, R. B.; Wallace, G. G. Processable Aqueous Dispersions of Graphene Nanosheets. *Nat. Nanotechnol.* **2008**, *3*, 101−105.
(13) Shan, C.; Yang, H.; Han, D.; Zhang, Q.; Ivaska, A.; Niu, L. Water-Soluble Graphene Covalently Functionalized by Biocompatible Poly-l-lysine. *Langmuir* **2009**, *25*, 12030−12033.
(14) Chen, K.; Chen, L.; Chen, Y.; Bai, H.; Li, L. Three-Dimensional Porous Graphene-Based Composite Materials: Electrochemical Synthesis and Application. *J. Mater. Chem.* **2012**, *22*, 20968−20976.
(15) Li, C.; Shi, G. Three-Dimensional Graphene Architectures. *Nanoscale* **2012**, *4*, 5549−5563.
(16) Chen, Z.; Ren, W.; Gao, L.; Liu, B.; Pei, S.; Cheng, H. Three-Dimensional Flexible and Conductive Interconnected Graphene Networks Grown by Chemical Vapour Deposition. *Nat. Mater.* **2011**, *10*, 424−428.
(17) Jung, I.; Young Jang, H.; Park, S. Direct Growth of Graphene Nanomesh Using A Au Nano-Network as A Metal Catalyst Via Chemical Vapor Deposition. *Appl. Phys. Lett.* **2013**, *103*, 023105/1−023405/5.
(18) Yi, J.; Lee, D. H.; Lee, W. W.; Park, W. I. Direct Synthesis of Graphene Meshes and Semipermanent Electrical Doping. *J. Phys. Chem. Lett.* **2013**, *4*, 2099−2104.
(19) Pettes, M. T.; Ji, H.; Ruoff, R. S.; Shi, L. Thermal Transport in Three-Dimensional Foam Architectures of Few-Layer Graphene and Ultrathin Graphite. *Nano Lett.* **2012**, *12*, 2959−2964.
(20) Korkut, S.; Roy-Mayhew, J. D.; Dabbs, D. M.; Milius, D. L.; Aksay, I. A. High Surface Area Tapes Produced with Functionalized Graphene. *ACS Nano* **2011**, *5*, 5214−5222.
(21) Choi, B. G.; Yang, M.; Hong, W. H.; Choi, J. W.; Huh, Y. S. 3D Macroporous Graphene Frameworks for Supercapacitors with High Energy and Power Densities. *ACS Nano* **2012**, *6*, 4020−4028.
(22) Chen, R.; Zhao, T.; Lu, J.; Wu, F.; Li, L.; Chen, J.; Tan, G.; Ye, Y.; Amine, K. Graphene-Based Three-Dimensional Hierarchical Sandwich-Type Architecture for High-Performance Li/S Batteries. *Nano Lett.* **2013**, *13*, 4642−4649.
(23) Wang, L.; Wang, D.; Zhang, F.; Jin, J. Interface Chemistry Guided Long-Cycle-Life Li-S Battery. *Nano Lett.* **2013**, *13*, 4206−4211.
(24) Wang, L.; Wang, D.; Dong, Z.; Zhang, F.; Jin, J. Interface Chemistry Engineering for Stable Cycling of Reduced GO/SnO_2 Nanocomposites for Lithium Ion Battery. *Nano Lett.* **2013**, *13*, 1711−1716.
(25) Zhang, L.; Zhao, X.; Stoller, M. D.; Zhu, Y.; Ji, H.; Murali, S.; Wu, Y.; Perales, S.; Clevenger, B.; Ruoff, R. S. Highly Conductive and Porous Activated Reduced Graphene Oxide Films for High-Power Supercapacitors. *Nano Lett.* **2012**, *12*, 1806−1812.
(26) Xu, Y.; Sheng, K.; Li, C.; Shi, G. Self-Assembled Graphene Hydrogel via a One-Step Hydrothermal Process. *ACS Nano* **2010**, *4*, 4324−4330.
(27) Hu, H.; Zhao, Z.; Wan, W.; Gogotsi, Y.; Qiu, J. Ultralight and Highly Compressible Graphene Aerogels. *Adv. Mater.* **2013**, *25*, 2219−2223.
(28) Worsley, M. A.; Pauzauskie, P. J.; Olson, T. Y.; Biener, J.; Satcher, J. H. J.; Baumann, T. F. Synthesis of Graphene Aerogel with High Electrical Conductivity. *J. Am. Chem. Soc.* **2010**, *132*, 14067−14069.
(29) Niu, Z.; Chen, J.; Hng, H. H.; Ma, J.; Chen, X. A Leavening Strategy to Prepare Reduced Graphene Oxide Foams. *Adv. Mater.* **2012**, *24*, 4144−4150.
(30) Jiang, X.; Ma, Y.; Li, J.; Fan, Q.; Huang, W. Self-Assembly of Reduced Graphene Oxide into Three-Dimensional Architecture by Divalent Ion Linkage. *J. Phys. Chem. C* **2010**, *114*, 22462−22465.
(31) Xiao, X.; Beechem, T. E.; Brumbach, M. T.; Lambert, T. N.; Davis, D. J.; Michael, J. R.; Washburn, C. M.; Wang, J.; Brozik, S. M.; Wheeler, D. R.; Burckel, D. B.; Polsky, R. Lithographically Defined Three-Dimensional Graphene Structures. *ACS Nano* **2012**, *6*, 3573−3579.
(32) Liang, Q.; Yao, X.; Wang, W.; Liu, Y.; Wong, C. P. A Three-Dimensional Vertically Aligned Functionalized Multilayer Graphene Architecture:An Approach for Graphene-Based Thermal Interfacial Materials. *ACS Nano* **2011**, *5*, 2392−2401.
(33) Ahn, H. S.; Jang, J.-W.; Seol, M.; Kim, J. M.; Yun, D.-J.; Park, C.; Kim, H.; Youn, D. H.; Kim, J. Y.; Park, G.; Park, S. C.; Kim, J. M.; Yu, D. I.; Yong, K.; Kim, M. H.; Lee, J. S. Self-Assembled Foam-Like Graphene Networks Formed through Nucleate Boiling. *Sci. Rep.* **2013**, *3*, 1396/1−1396/8.
(34) Pettes, M. T.; Jo, I.; Yao, Z.; Shi, L. Influence of Polymeric Residue on the Thermal Conductivity of Suspended Bilayer Graphene. *Nano Lett.* **2011**, *11*, 1195−1200.
(35) Ahn, Y.; Kim, H.; Kim, Y.-H.; Yi, Y.; Kim, S.-I. Procedure of Removing Polymer Residues and Its Influences on Electronic and Structural Characteristics of Graphene. *Appl. Phys. Lett.* **2013**, *102*, 091602/1−091602/6.
(36) Li, W.; Gao, S.; Wu, L.; Qiu, S.; Guo, Y.; Geng, X.; Chen, M.; Liao, S.; Zhu, C.; Gong, Y.; Long, M.; Xu, J.; Wei, X.; Sun, M.; Liu, L. High-Density Three-Dimension Graphene Macroscopic Objects for High-Capacity Removal of Heavy Metal Ions. *Sci. Rep.* **2013**, *3*, 2125/1−2125/6.
(37) Dreyer, D. R.; Park, S.; Bielawski, C. W.; Ruoff, R. S. The Chemistry of Graphene Oxide. *Chem. Soc. Rev.* **2010**, *39*, 228−240.
(38) Zhu, Y.; James, D. K.; Tour, J. M. New Routes to Graphene, Graphene Oxide and Their Related Applications. *Adv. Mater.* **2012**, *24*, 4924−4955.
(39) Zhu, Y.; Murali, S.; Cai, W.; Li, X.; Suk, J. W.; Potts, J. R.; Ruoff, R. S. Graphene and Graphene Oxide: Synthesis, Properties, and Applications. *Adv. Mater.* **2010**, *22*, 3906−3924.
(40) Wang, Z.; Xu, D.; Huang, Y.; Wu, Z.; Wang, L.; Zhang, X. Facile, Mild and Fast Thermal-Decomposition Reduction of Graphene Oxide in Air and Its Application in High-Performance Lithium Batteries. *Chem. Commun.* **2012**, *48*, 976−978.
(41) Mao, S.; Pu, H.; Chen, J. Graphene Oxide and Its Reduction: Modeling and Experimental Progress. *RSC Adv.* **2012**, *2*, 2643−2662.
(42) Gilje, S.; Dubin, S.; Badakhshan, A.; Farrar, J.; Danczyk, S. A.; Kaner, R. B. Photothermal Deoxygenation of Graphene Oxide for Patterning and Distributed Ignition Applications. *Adv. Mater.* **2010**, *22*, 419−423.
(43) Wei, W.; He, T.; Teng, X.; Wu, S.; Ma, L.; Zhang, H.; Ma, J.; Yang, Y.; Chen, H.; Han, Y.; Sun, H.; Huang, L. Nanocomposites of Graphene Oxide and Upconversion Rare-Earth Nanocrystals with Superior Optical Limiting Performance. *Small* **2012**, *8*, 2271−2276.
(44) Paredes, J. I.; Villar-Rodil, S.; Martinez-Alonso, A.; Tascon, J. M. D. Graphene Oxide Dispersions in Organic Solvents. *Langmuir* **2008**, *24*, 10560−10564.
(45) Karousis, N.; Economopoulos, S. P.; Sarantopoulou, E.; Tagmatarchis, N. Porphyrin Counter Anion in Imidazolium-Modified Graphene-Oxide. *Carbon* **2010**, *48*, 854−860.
(46) Karousis, N.; Sandanayaka, A. S. D.; Hasobe, T.; Economopoulos, S. P.; Sarantopoulou, E.; Tagmatarchis, N. Graphene Oxide with Covalently Linked Porphyrin Antennae: Synthesis, Characterization and Photophysical Properties. *J. Mater. Chem.* **2011**, *21*, 109−117.
(47) Lee, H. B.; Raghu, A.; Yoon, K. S.; Jeong, H. M. Preparation and Characterization of Poly(ethylene oxide)/Graphene Nanocomposites from an Aqueous Medium. *J. Macromol. Sci., Part B: Phys.* **2010**, *49*, 802−809.
(48) Sun, X.; Liu, Z.; Welsher, K.; Robinson, J. T.; Goodwin, A.; Zaric, S.; Dai, H. Nano-Graphene Oxide for Cellular Imaging and Drug Delivery. *Nano Res.* **2008**, *1*, 203−212.
(49) Zhu, J.; Li, Y.; Chen, Y.; Wang, J.; Zhang, B.; Zhang, J.; Blau, W. J. Graphene Oxide Covalently Functionalized with Zinc Phthalocyanine for Broadband Optical Limiting. *Carbon* **2011**, *49*, 1900−1905.

DOI: 10.1021/am508909h
ACS Appl. Mater. Interfaces 2015, 7, 1057−1064

(50) Yu, G.; Hu, L.; Vosgueritchian, M.; Wang, H.; Xie, X.; McDonough, J. R.; Cui, X.; Cui, Y.; Bao, Z. Solution-Processed Graphene/MnO_2 Nanostructured Textiles for High-Performance Electrochemical Capacitors. *Nano Lett.* **2011**, *11*, 2905−2911.
(51) Peterson, G. R.; Cychosz, K. A.; Thommes, M.; Hope-Weeks, L. J. Solvent-Tuned Hierarchical Porosity in Nitrocellulose Aerogels. *Chem. Commun.* **2012**, *48*, 11754−11756.
(52) Tanyolac, D.; Ozdural, A. R. Preparation of Low-Cost Magnetic Nitrocellulose Microbeads. *React. Funct. Polym.* **2000**, *45*, 235−242.
(53) Zhang, X.; Zhang, G.; Liao, Y.-C.; Weeks, B. L.; Zhang, Z. Embossing of Organic Thin Films Using a Surfactant Assisted Lift-Off Technique. *J. Colloid Interface Sci.* **2012**, *387*, 175−179.
(54) Pourmortazavi, S. M.; Hosseini, S. G.; Rahimi-Nasrabadi, M.; Hajimirsadeghi, S. S.; Momenian, H. Effect of Nitrate Content on Thermal Decomposition of Nitrocellulose. *J. Hazard. Mater.* **2009**, *162*, 1141−1144.
(55) Wei, W.; Jiang, X.; Lu, L.; Yang, X.; Wang, X. Study on The Catalytic Effect of NiO Nanoparticles on the Thermal Decomposition of TEGDN/NC Propellant. *J. Hazard. Mater.* **2009**, *168*, 838−842.
(56) Zhang, X.; Weeks, B. L. Preparation of Sub-micron Nitrocellulose Particles for Improved Combustion Behavior. *J. Hazard. Mater.* **2014**, *268*, 224−228.
(57) Zhang, X.; Hikal, W. M.; Zhang, Y.; Bhattacharia, S. K.; Li, L.; Panditrao, S.; Wang, S.; Weeks, B. L. Direct Laser Initiation and Improved Thermal Stability of Nitrocellulose/Graphene Oxide Nanocomposites. *Appl. Phys. Lett.* **2013**, *102*, 141905/1−141905/5.
(58) Van Der Pauw, L. J. A Method of Measuring The Resistivity and Hall Coefficient on Lamellae of Arbitrary Shape. *Philips Tech. Rev.* **1958**, *20*, 220−224.
(59) Yang, D.; Velamakanni, A.; Bozoklu, G.; Park, S.; Stoller, M.; Piner, R. D.; Stankovich, S.; Jung, I.; Field, D. A.; Ventrice, C. A.; Ruoff, R. S. Chemical Analysis of Graphene Oxide Films after Heat and Chemical Treatments by X-ray Photoelectron and Micro-Raman Spectroscopy. *Carbon* **2009**, *47*, 145−152.
(60) Wang, H.; Maiyalagan, T.; Wang, X. Review on Recent Progress in Nitrogen-Doped Graphene: Synthesis, Characterization, and Its Potential Applications. *ACS Catal.* **2012**, *2*, 781−794.
(61) Stankovich, S.; Dikin, D. A.; Piner, R. D.; Kohlhaas, K. A.; Kleinhammes, A.; Jia, Y.; Wu, Y.; Nguyen, S. T.; Ruoff, R. S. Synthesis of Graphene-Based Nanosheets Via Chemical Reduction of Exfoliated Graphite Oxide. *Carbon* **2007**, *45*, 1558−1565.
(62) Zhang, J.; Yang, H.; Shen, G.; Cheng, P.; Zhang, J.; Guo, S. Reduction of Graphene Oxide Via L-Ascorbic Acid. *Chem. Commun.* **2010**, *46*, 1112−1114.
(63) Li, L.; Zhang, X.; Qiu, J.; Weeks, B. L.; Wang, S. Reduced Graphene Oxide-Linked Stacked Polymer Forests for High Energy-Density Supercapacitor. *Nano Energy* **2013**, *2*, 628−635.

DOI: 10.1021/am508909h
ACS Appl. Mater. Interfaces 2015, 7, 1057−1064